Dynamic diffractive resonant radiation in a linearly chirped nonlinear waveguide array

Anuj P. Lara
Department of Physics, Indian Institute of Technology Kharagpur, Kharagpur 721302, India

Samudra Roy*
Department of Physics, Indian Institute of Technology Kharagpur, Kharagpur 721302, India
and Centre of Theoretical Studies, Indian Institute of Technology Kharagpur, Kharagpur 721302, India

(Received 22 May 2020; accepted 18 August 2020; published 14 September 2020)

We theoretically and numerically investigate the evolution of a discrete soliton in a semi-infinite linearly chirped one-dimensional nonlinear waveguide array (WA). The discrete soliton is self-accelerated inside the transversely chirped WA and emits a *dynamic diffractive resonant radiation* (DifRR). The radiation appears when the soliton wave number is matched with the linear radiation wave. Unlike the uniform WA, the DifRR can be excited even for zero wave number of the input soliton when the waveguide channels are chirped. The transverse modulation due to chirp conceptually imposes a linear potential which acts as a perturbation to soliton dynamics and leads to a monotonous wave-number shift of the propagating wave. Exploiting perturbative variational analysis we determine the equation of motion of the soliton wave number and use it to establish a modified phase-matching condition which takes into account the soliton wave-number shift and efficiently predicts the dynamic DifRR. A startling effect like generation of dual DifRR occurs as a result of the interplay between the self-accelerated soliton and its initial wave number. We exploit the modified phase-matching relation to understand this unique phenomenon of dual radiation and find a satisfactory agreement with numerical results in radiation wave-number calculation.

DOI: 10.1103/PhysRevA.102.033512

I. INTRODUCTION

Waveguide arrays (WAs) since their first inception [1] have provided a strong platform to study discrete phenomena which are fundamental in nature. In a WA, a large number (infinite in principle) of single-mode waveguide channels are placed periodically such that their individual modes overlap and the evolution of an optical field can be represented as a discrete problem. Periodic photonic structures can afford additional control of light, making it possible to explore new physical regimes that are forbidden in homogeneous systems. Discrete diffraction [2], discrete solitons [3,4], and their interaction with the periodic refractive index lattice are a few examples of light management studied in great detail in past years [5]. For a discrete soliton, a transverse index array is analogous to the continuous temporal counterpart of an optical soliton excited in an optical fiber. The discrete nature of the spatial soliton introduces additional exciting properties to their characteristics like the Peierls-Nabarro potential [6], Bloch oscillations [7], and Anderson localization [8]. Modulation of the periodic structure in a uniform homogeneous WA provides additional degrees of freedom in terms of a binary WA which offers richer optical properties. Binary arrays which are composed of waveguides with different wave numbers allow us to appreciate an optical approach to study relativistic phenomena such as Bloch-Zener oscillations [9], *Zitterbewegung* [10], Dirac solitons [11], and neutrino oscillations [12], to name a few. In addition, introduction of an amplitude and frequency modulation in the WA has been used to implement beam steering or routing [13,14] and formation of surface solitons [15]. Further extending these phenomena in the plasmonic regime with beam focusing in a metallic WA [16], and plasmonic Bloch oscillations in metal-dielectric and graphene arrays [17,18], proves the versatility of this system. In homogeneous WAs, discrete solitons arise due to the stable balance of discrete diffraction and self focusing originating from Kerr nonlinearity. The evolution of electric fields in these WAs is given by the coupled-mode equations which describe the dynamics of the modes in individual waveguides. These equations take into account the self-propagation of a field in a waveguide, both linear and nonlinear, as well as the interwaveguide interactions that take place through the coupling of the modes by the evanescent electric fields. Although different properties of these discrete solitons have been studied over the years, the phenomenon of these solitons emitting a radiation is a comparatively recent development [19] in this field. This radiation, aptly named *diffractive resonant radiation* (DifRR)[19], is emitted by a special soliton propagating in a uniform WA. Such radiation is the spatial (or wave-number) analog to dispersive radiation emitted from an ultrashort pulse in an optical fiber [20]. The presence of higher-order dispersion in fibers leads to a phase-matching (PM) situation which allows the soliton to transfer energy to the linear dispersive waves at specific frequencies. Similar to its temporal counterpart, static DifRR having a specific wave number is emitted when the soliton wave number matches with the linear wave propagating in a WA. However, the Brillouin boundary due to the one-dimensional (1D) lattice created by the periodic arrangement of waveguides limits the possible wave numbers to lie within $-\pi$ and π. Any electric

*samudra.roy@phy.iitkgp.ac.in

field going beyond this boundary undergoes a 2π shift and emerges from the other side of the boundary. This unusual effect is termed as *anomalous recoil* [19]. We will see in the later sections that an initial wave number is required to generate the DifRR [19] whereas it can be controlled by some other parameters like soliton power and coupling coefficient.

In this paper we mainly investigate the dynamics of DifRR emitted by a discrete soliton in a geometrically modified nonuniform WA. A modification in WA provides a versatile platform for controlling light where a propagating optical field experiences perturbation. An instability can be introduced to perturb the optical field by providing external irregularities in the WA by modifying either the refractive index or the waveguide arrangement. A constant difference of the propagation vector in the adjacent channel arises due to the transverse index gradient showing exciting dynamics even in the linear domain where an optical analogy of Bloch oscillations is identified [21,22]. In another scheme, the coupling coefficients of the WA are randomly varied by changing their relative positions of waveguide channels, which offers Anderson localization [23]. Inspired by these works we make an attempt to understand the optical field dynamics inside a linearly chirped 1D WA, which is less explored in the context of discrete soliton propagation. In a linearly chirped WA the separation between adjacent waveguides increases (or decreases) with a uniform rate called the *chirp parameter* which leads to a variation in the coupling coefficient. DifRR becomes an inevitable phenomenon in the chirped WA where the soliton moves with a self-accelerated mode. The DifRR is found to be dynamic in nature where radiation wave number shifts along propagation distance. One can appreciate a similarity of this phenomenon with the dispersive wave generation in tapered fibers during the supercontinuum process [24–27]. The tapered fiber where the dispersion profile varies along fiber length exhibits a radiation which drifts away in the frequency domain and is trapped by the soliton [28]. The phase-matching condition changes with propagation distance owing to the longitudinal variation of dispersion and eventually leads to a radiation the frequency of which shifts along propagation. For the nonuniform WA the chirp conceptually acts as a linear potential that perturbs the soliton propagation and leads to dynamic DifRR. The soliton dynamics under the linear potential is theoretically estimated exploring perturbative analysis based on variational theory. Exploring these results we establish a modified PM expression which predicts the dynamic DifRR accurately for the chirped WA. Further we extend our investigation to DifRR formation under nonzero initial soliton wave number ($k_0 \neq 0$). The interplay between the chirp parameter and k_0 opens up an operational domain previously not possible. Here we find an interesting case for $k_0 > 0$ where dual DifRR appears, which is analogous to the dual dispersive wave emission occurring in the temporal domain for two-zero dispersion waveguides [29]. Based on theoretical analysis we try to explain the intriguing effect of dual DifRR, and the agreement between numerical and analytical results is satisfactory.

II. THEORY

A semi-infinite array of identical periodic nonlinear waveguides with no losses is considered as ideal WAs. For

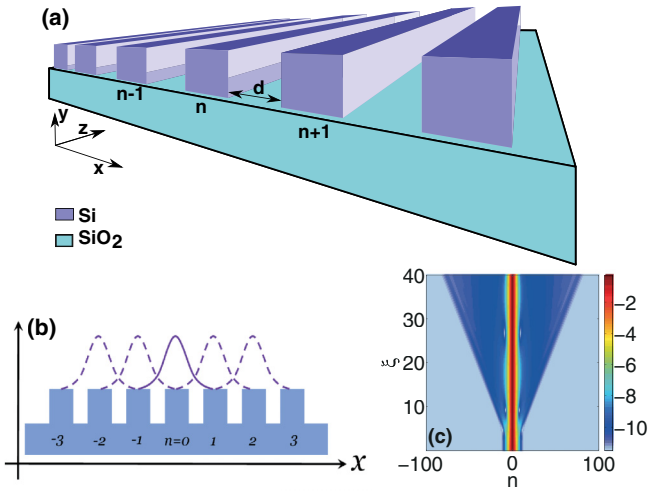

FIG. 1. (a) A uniform WA having interwaveguide separation d. (b) Schematic representation of nearest-neighbor evanescent mode coupling. (c) Formation of a discrete soliton in a nonlinear WA.

continuous-wave excitation in such WA, the evolution of mode amplitude in the nth waveguide with nearest-neighbor evanescent coupling is described by the discrete nonlinear Schrödinger equation (DNLSE) [30–32]:

$$i\frac{dE_n}{dz} + C_{(n)}^{(n+1)}E_{(n+1)} + C_{(n)}^{(n-1)}E_{(n-1)} + \gamma|E_n|^2E_n = 0. \quad (1)$$

E_n is the electric-field amplitude of the nth waveguide. If the total number of waveguides is considered as $(2N+1)$ then the index n ranges from $-N \leqslant n \leqslant N$. Here, $C_{(n)}^{(n+1)}$ and $C_{(n)}^{(n-1)}$ are, respectively, the coupling coefficients of the $(n+1)$th and $(n-1)$th waveguides to the nth waveguide in units of 1/m. $\gamma = \omega_0 n_2/(cA_{\text{eff}})$ is the nonlinear coefficient of a single waveguide in units of 1/W m where n_2 is the Kerr coefficient and A_{eff} is the effective area of the modes. In Fig. 1(a) we represent the model of a uniform WA having equal separation between the two consecutive waveguide channels. The coupling coefficients which are a function of separation become identical throughout the WA ($C_{(n)}^{(n+1)} = C_{(n)}^{(n-1)} = C$). The nearest-neighbor evanescent mode coupling is schematically illustrated in Fig. 1(b) where the sketch of the refractive index in the lattice is shown. At low powers the nonlinear term can be neglected ($\gamma = 0$) and Eq. (1) can be analytically integrable. A single waveguide excitation leads to a solution $E_n(z) = E_n(0)i^nJ_n(2Cz)$ exhibiting discrete diffraction [4], where J_n is the Bessel function of order n. Physically, the discrete diffraction is originated due to the varying z-dependent phase shift for different transverse wave-vector components. The discrete diffraction can be restricted by the focusing nonlinearity of the system and one can intuitively understand the soliton formation as a balance between Kerr nonlinearity and diffraction. In Fig. 1(c) we demonstrate a discrete soliton that is originated in the uniform nonlinear WA. For the uniform WA [Fig. 1(a)] a useful normalized form of the DNLSE can be realized by making the transformations

$E_n \to \sqrt{P_0}\psi_n$, $\gamma P_0 z \to \xi$, and $C/(\gamma P_0) \to c$:

$$i\frac{d\psi_n}{d\xi} + c[\psi_{n+1} + a_{n-1}] + |\psi_n|^2\psi_n = 0, \tag{2}$$

where P_0 is the peak power of the associated beam in units of W. Note, the total power $P = \sum_n |\psi_n|^2$ and Hamiltonian $H = \sum_n [c|\psi_n - \psi_{n-1}|^2 - \frac{\gamma}{2}|\psi_n|^4]$ remain conserved during propagation [31]. For a stationary discrete plane-wave solution $\psi_n(\xi) = \psi_0 \exp[i(nk_x d + \beta\xi)]$ of Eq. (2), one can obtain the dispersion relation between β and k_x as [33]

$$\beta(\kappa) = 2c\cos(\kappa) + |\psi_0|^2, \tag{3}$$

where d is the separation between two adjacent waveguide, k_x is the transverse wave vector, and $\kappa = k_x d$ represents the phase difference between adjacent waveguides. Note, during propagation the transverse component (κ) gains a phase $\phi_t = \beta(\kappa)\xi$ which leads to the transverse shift $\Delta n = \partial\phi_t/\partial\kappa$ of the propagating beam [34]. The angle θ of beam propagation follows $\tan\theta = \Delta n/\xi$. Hence κ governs the propagation direction as $\theta = \tan^{-1}[\partial\beta(\kappa)/\partial\kappa] = \tan^{-1}[-2c\sin(\kappa)]$ [35]. The Taylor expansion of $\beta(\kappa)$ about the incident wave number (κ_0) gives us an expanded diffraction relation:

$$\beta(\kappa) = \beta(\kappa_0) + \sum_{m\geqslant 1}\frac{D_m}{m!}\Delta\kappa^m, \tag{4}$$

where $D_m \equiv (d^m\beta/d\kappa^m)|_{\kappa_0}$ and $\Delta\kappa = \kappa - \kappa_0$. The Fourier transformation to change the domain $\kappa \to n$ is done by replacing $\Delta\kappa \equiv -i\partial_n$ where n is defined as a continuous variable of an amplitude function $\Psi(n,\xi) = \psi_{n,\xi}\exp(-i\kappa_0 n)$ [2,5].

Defining n as a continuous variable, which is justified as solitons extend for several waveguides, we have an approximated standard nonlinear Schrödinger equation (NLSE) [19]:

$$\left[i\partial_\xi - \frac{D_2}{2}\partial_n^2 + \sum_{m\geqslant 3}\frac{D_m}{m!}(-i\partial_n)^m + |\Psi(n,\xi)|^2\right]\Psi(n,\xi) = 0. \tag{5}$$

The first and second terms of the Taylor expansion are eliminated by introducing a phase evolution substitution $\Psi(n,\xi) \to \Psi(n,\xi)\exp[i\beta(\kappa_0)\xi]$ and using the concept of comoving frame $n \to n + D_1\xi$. For $D_{m\geqslant 3} = 0$, Eq. (5) has a soliton solution given by

$$\Psi_{\rm sol} = \Psi_0 \mathrm{sech}\left(\frac{n\Psi_0}{\sqrt{|D_2|}}\right)\exp(ik_{\rm sol}\xi), \tag{6}$$

where $k_{\rm sol} \equiv \Psi_0^2/2$ is the longitudinal wave number for the spatial soliton. Note that for the bright soliton solution we have the condition $|\kappa_0| < \pi/2$. The plane-wave solution $\exp[i(k_{\rm lin}\xi + \Delta\kappa n)]$ of the linearized Eq. (5) gives us the dispersion relation:

$$k_{\rm lin}(\Delta\kappa) = \beta(\kappa) - \beta(\kappa_0) - D_1\Delta\kappa. \tag{7}$$

A soliton of the form given by Eq. (6) transfers energy to the linear wave and generates a radiation when $k_{\rm sol} = k_{\rm lin}(\Delta\kappa)$ is satisfied. This is the required PM condition for the DifRR as predicted in the seminal paper [19].

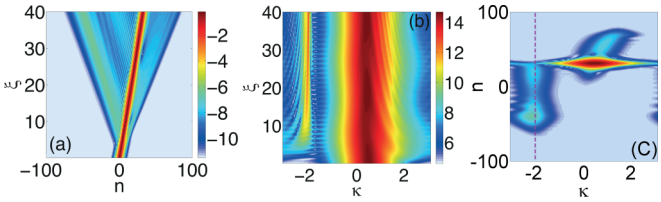

FIG. 2. Discrete soliton propagation in (a) n space and (b) κ space for $\psi_0 = 0.8$ and $\kappa_0 = 0.5$. (c) Spatial spectrogram at $\xi = 40$ where diffractive radiation is evident. The vertical dotted line indicates the location of $\kappa_{\rm RR}$ which is obtained by solving Eq. (8).

Generation of diffractive resonant radiation in a uniform waveguide array

The generation of DifRR requires the soliton to have an initial wave number as per the phase-matching equation. The PM condition $k_{\rm sol} = k_{\rm lin}(\Delta\kappa)$ leads to a transcendental equation:

$$[\cos(\kappa) - \cos(\kappa_0) + \sin(\kappa_0)\Delta\kappa] = \widetilde{\Psi}_0^2, \tag{8}$$

where $\widetilde{\Psi}_0 = \Psi_0/2\sqrt{c}$. The solution of this relation gives the wave number of the generated DifRR ($\kappa_{\rm RR} = \kappa_0 + \Delta\kappa$) as a function of initial soliton wave number κ_0. Considering the contribution of the right-hand side is small one can have an approximate solution of Eq. (8):

$$\kappa_{\rm RR} \approx \kappa_0 + 3\cot(\kappa_0)\left[1 - \tfrac{1}{4}(1 - \sqrt{1+\Delta^2})\right], \tag{9}$$

where $\Delta = \frac{4\widetilde{\Psi}_0}{3}\frac{\tan\kappa_0}{\sqrt{\cos\kappa_0}}$. The approximated solution is valid under a certain range of parameters and consistent with the result given in [19] if we neglect Δ. In Fig. 2 we demonstrate the dynamics of the soliton and the formation of DifRR in a uniform WA. The evolution of the input beam with the form $\Psi_{\rm sol} = \Psi_0\mathrm{sech}(n\Psi_0/\sqrt{|D_2|})e^{ik_{\rm sol}\xi}$ is shown in Fig. 2(a). The soliton emits radiation around $\xi = 5$ as demonstrated in the Fourier spectrum of $\Psi(n)$ in Fig. 2(b). The spatial spectrogram in (n-κ) space is shown in Fig. 2(c) where the location of the DifRR ($\kappa_{\rm RR}$) is indicated by the vertical dotted line. The spectrogram is a well-known technique through which we can plot the position and its spatial counterpart wave number together.

Mathematically it is defined as $\mathcal{S}(n,\kappa,\xi) = |\int_\infty^\infty \Psi(n',\xi)\Psi_{\rm ref}(n-n')e^{i\kappa n'}dn'|^2$ where $\Psi_{\rm ref}$ is the reference window function normally taken as the input. Equation (8) is exploited to estimate the location of $\kappa_{\rm RR}$ in κ space. Note, the limit of the κ domain lies within the first Brillouin zone ($-\pi < \kappa < \pi$) and if any part of the soliton or DifRR crosses this limit an additional wave number of -2π gets added. The Brillouin boundary appears due to the 1D lattice formed by the periodic arrangement of waveguides. This confines the value of the wave number to this limit, and the phenomenon is termed as *anomalous recoil* [19,36].

From the phase-matching equation Eq. (8), it is evident that DifRR can be tunable under various parameters like initial soliton wave number or momentum (κ_0), coupling coefficient (c), and beam amplitude (Ψ_0). In the previous studies [19,36] the dominant role of input wave number (κ_0) is mainly investigated in the context of DifRR formation. The approximate closed-form expression $\kappa_{\rm RR} = \kappa_0 + 3/\tan\kappa_0$ is proposed to deduce the wave number of DifRR. In this paper, however, we

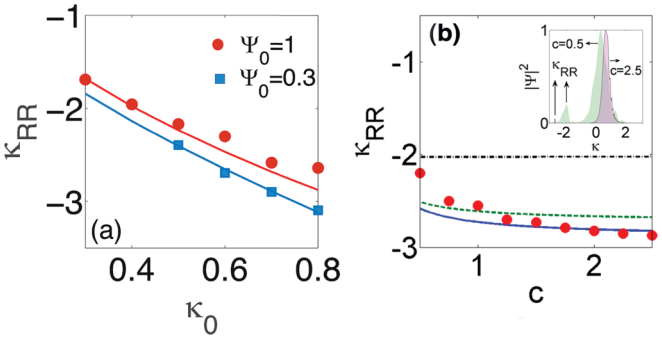

FIG. 3. (a) Location of DifRR (κ_{RR}) as a function of input soliton wave number κ_0 for two different amplitudes. Numerically obtained κ_{RR} are presented by solid dots and squares. The solid lines based on the solution of Eq. (8) theoretically predict κ_{RR}. (b) Variation of κ_{RR} as a function of coupling constant (c). The solid dots are numerical data where the solid line represents the PM solution of Eq. (8). The dashed line corresponds to the closed-form expression shown in Eq. (9). The horizontal dot-dashed line appears when we neglect Δ in Eq. (9). In the inset we show the formation of DifRR for two different coupling constants.

try to generalize the study by capturing the role of two other parameters Ψ_0 and c in the evolution of DifRR. In Fig. 3(a) we plot the DifRR wave number as a function of κ_0 for two different beam amplitudes. We find there is a difference in κ_{RR} values when we change beam amplitude. The full PM expression Eq. (8) (solid lines) nicely predicts the DifRR wave number in both cases. Next we examine the role of the coupling coefficient in DifRR generation. Note, the coupling coefficient can be easily varied by changing the separation between waveguide channels. In Fig. 3(b) we illustrate the variation of DifRR wave number (κ_{RR}) with coupling coefficient c. The solid dots represent the values of κ_{RR} which are obtained numerically by solving Eq. (2) whereas the solid line corresponds to the PM solution of Eq. (8). The dashed line represents the approximated closed expression derived in Eq. (9). For a comparison we also plot (horizontal dot-dashed line) the closed-form expression $\kappa_{RR} = \kappa_0 + 3/\tan\kappa_0$ derived in [19]. In the inset we show the field distribution $|\Psi_0|^2$ in k space for two different c values where the shift of the radiation is evident. It is also noticed that a stronger but wide radiation emerges for low values of coupling coefficient c whereas a sharp but weak radiation appears when c is comparatively large. We find for low coupling coefficients that numerically it is tricky to determine the exact value of κ_{RR} as the radiation spreads over a region. This anomaly in measurement causes a slight deviation in numerical and analytical results especially for low c values.

III. DISCRETE SOLITON IN A CHIRPED WAVEGUIDE ARRAY

The propagation dynamics of the discrete soliton becomes more intriguing and practically useful if some nonuniformity is introduced in the WA. Depending on the application, a few standard strategies are implemented to bring nonuniformity in WAs, such as changing the waveguide width [8] or changing the separation between adjacent waveguides [23]. Such WAs are used to describe the Anderson localization in nonlinear optics. In another scheme, optical Bloch oscillations can be realized in WAs with linear refractive index modulation in the transverse direction [21]. The linear refractive index variation is mathematically adjusted by incorporating a linear potential term in the NLSE. In this paper, we have introduced a chirped WA where the separation between adjacent waveguides changes linearly. The coordinate of the nth waveguide is defined as $x_n = nd_0 + \frac{\delta}{2}n(n-1)$, where d_0 is the separation between central ($n = 0$) and first ($n = 1$) waveguides and δ defines the increment of waveguide separation in real units. We introduce a normalized chirp parameter defined by $g_c = \delta/d_0$ that denotes the strength of chirping where the relative separation between adjacent waveguides is defined by $d_n = d_0(1 + ng_c)$. Note, for a linearly chirped WA the upper limit of the waveguide number ($2N_{max} + 1$) can be estimated by simply setting the geometric restriction that the lowest separation between two adjacent waveguides is zero ($d_n = 0$). This condition allows us to estimate $N_{max} = g_c^{-1}$. For a linearly chirped WA, the propagation constant remains the same for all waveguide channels while the coupling coefficient (c) varies along transverse distance. A linearly chirped WA is conceptually realized by a linear potential [37]. Exploiting this concept we may configure a perturbed NLSE as $[i\partial_\xi + \frac{1}{2}\partial_n^2 + |\Psi(n,\xi)|^2]\Psi(n,\xi) = \frac{i}{2}\epsilon$, where $\epsilon = i\chi n\Psi$ accounts for the linear potential term as a perturbation and χ is related to the potential strength. A standard perturbative variational analysis [38] with a regular ansatz, $\Psi = \eta\,\mathrm{sech}[\eta(n-n_0)]e^{i[\phi-\kappa(n-n_0)]}$, can be exploited to estimate the evolution of the soliton wave number (κ) and position (n_0) under linear potential. The variational treatment ensures the conservation of total energy $\frac{\partial\mathcal{E}}{\partial\xi} = 0$, ($\mathcal{E} = \int|\Psi|^2 dn$) and leads to the equation of motions, $\frac{\partial\kappa}{\partial\xi} = -\chi$ and $\frac{\partial n_0}{\partial\xi} = \kappa$. While propagating through a uniform WA ($\epsilon = 0$), the soliton maintains its wave number. However, an evolution in the wave number is implemented when the soliton propagates under perturbation like a linear potential appearing transversely along the n coordinate which takes into account the chirping. The variational result predicts that the soliton wave number starting at κ_0 experiences a continuous linear shift $\kappa(\xi) = \kappa_0 - \chi\xi$. The corresponding evolution in the position of the soliton is $n_0(\xi) = n_0(0) - \frac{1}{2}\chi\xi^2$ when starting with $\kappa_0 = 0$. A similar evolution of the soliton is observed in a WA with quasiperiodic lattice arrangement [39], which suggests the idea of DifRR generation in such systems.

A. Waveguide design

Before going into a detailed analysis of soliton dynamics it is important to define a physically realizable waveguide structure that supports DifRR. Strategically, a chirped WA can be formed by modulating either the refractive index of waveguide channels or their relative separation. Modulation of the refractive index introduces a position dependent propagation vector, while modification of the waveguide separation results in a position dependent coupling coefficient. The facility of fs laser based writing in a transparent bulk medium [40,41] allows us to design a WA of cores suspended in its cladding as modeled in Fig. 4(a). We propose GeO_2 doped silica cores suspended in a silica cladding, to have an equivalent refractive index

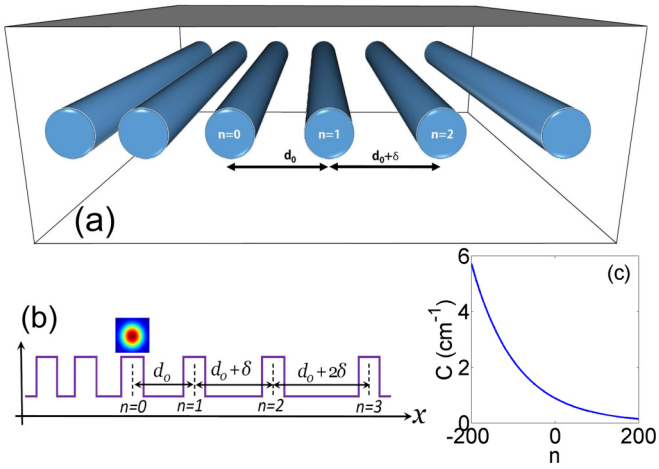

FIG. 4. (a) Pictorial model of the proposed chirped WA where the cylindrical channels are placed nonuniformly with increasing separation. The separation between adjacent waveguide channels is $d_n = (d_0 + n\delta)$, where $-N \leqslant n \leqslant N$. (b) Schematic representation of the waveguide arrangement where the central channel ($n = 0$) is illuminated by the input electric field. (c) Spatial variation of the coupling coefficient in real units.

difference Δn, between the core and cladding. At operating wavelength $\lambda_0 = 1.55\ \mu$m, the core and cladding refractive indices are $n_1 \approx 1.4477$ and $n_2 \approx 1.4446$, respectively. We consider the radius of the cylindrical core $a = 5\,\mu$m. For the given geometry of the WA the nonlinear coefficient is calculated as $\gamma = 0.79\ \mathrm{W^{-1}\,km^{-1}}$. As schematically shown in Fig. 4(b), a chirped WA is designed by taking an initial separation d_0= 20 μm between the central reference waveguide ($n = 0$) and $n = 1$ waveguide, then applying a progressive change in separation (δ) in the nm range to keep the resulting perturbation small. Since the separation between waveguides is a function of position, we calculate the coupling coefficients as a function of the respective separation (d_n) using [42]

$$C(d_n) = \frac{\lambda_0}{2\pi n_1}\frac{U^2}{a^2V^2}\frac{K_0(W d_n/a)}{K_1^2(W)}. \tag{10}$$

Here $d_n = d_0(1 + ng_c)$; λ_0 is the wavelength in free space (1.55 μm in this case); n_1 and n_2 are the core and cladding refractive indices, respectively; a is the core radius; and K_v are the modified Bessel functions of the second kind of order v. U and V are the mode parameters that satisfy $U^2 + W^2 = V^2$, where the V parameter is defined by $V = \frac{2\pi a}{\lambda_0}\sqrt{n_1^2 - n_2^2}$. U is given approximately as $U \cong 2.405e^{-(1-v/2)/V}$, with $v = 1 - (n_2/n_1)^2$ [43]. In Fig. 4(c) we depict the variation of the coupling coefficient (C) in real units for the proposed chirped WA.

B. Generation of dynamic DifRR in a linearly chirped waveguide array

In this section we numerically investigate the evolution of a discrete soliton Eq. (6) in a linearly chirped WA and formation of dynamics DifRR. We can construct a normalized set of DNLSEs from Eq. (1) by taking the transformations $\eta_n^{n\pm1} \to C_{(n)}^{(n\pm1)}/C_0$, $\xi \to C_0 z$, $E_n \to \sqrt{P_0}a_n$, and $\psi_n \to \psi_0 a_n$,

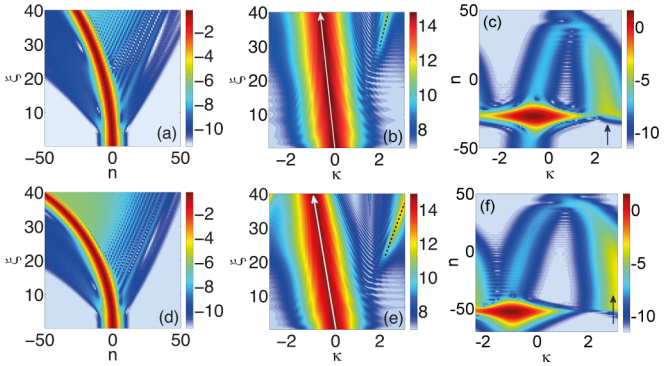

FIG. 5. Discrete soliton propagation in the (a), (d) (n-ξ) and (b), (e) (κ-ξ) plane for $\psi_0 = 0.8$, $\kappa_0 = 0$, and δ=30 nm [for (a) and (b)] and δ=50 nm [for (d) and (e)]. Dynamic DifRR is evident in κ space. (c), (f) Spatial spectrogram at $\xi = 40$ where DifRR is indicated by arrows.

where $\psi_0 \to \sqrt{\gamma P_0/C_0}$:

$$i\frac{d\psi_n}{d\xi}(\xi) + \eta_{(n)}^{(n+1)}\psi_{n+1}(\xi) + \eta_{(n)}^{(n-1)}\psi_{n-1}(\xi) + |\psi_n(\xi)|^2\psi_n(\xi) = 0. \tag{11}$$

Here C_0 is the coupling coefficient between the central ($n = 0$) and first ($n = 1$) waveguide channel the value of which is calculated to be $\approx$1 cm^{-1}. Equation (11) mathematically describes the soliton evolution in the chirped WA. In a preliminary analysis, we numerically investigate the dynamics of the soliton inside the proposed WA, which is schematically shown in Fig. 4(a). We launch Eq. (6), which is the approximate soliton-solution in the continuous limit, in a discrete photonic system where the coupling coefficient varies along the direction transverse to the propagation direction. The value of g_c determines the rate at which the coupling coefficient changes. It is apparent from Eq. (10) that the value of the coupling coefficient (C) will decrease as the separation increases owing to the decaying nature of the modified Bessel function of second kind $K_j(x)$. The value of δ is considered small ($\approx$nm) compared to the separation ($\approx\mu$m) between waveguides. The power scale $P_0 \sim 125$ kW makes the scaling factor ψ_0 to unity and length scale become $\approx$1 cm. In Fig. 5 we demonstrate the propagation of the discrete soliton for two different values of δ by numerically solving the governing equation Eq. (11). In the simulation, the total number of waveguide channels is considered to be ($2N + 1 = 701$) with the range of n index as $-350 \leqslant n \leqslant 350$. We observe that for nonzero δ the soliton changes its wave number linearly along its propagation [see Figs. 5(a) and 5(d)] and experiences an accelerated motion in the spatial (n) domain [see Figs. 5(b) and 5(e)] which is quite different from what we observed in the uniform WA. The rate of wave-number shift and spatial acceleration is increased as the value of δ is increased. In Figs. 5(b) and 5(e) the arrows indicate the linear shift of soliton wave number κ due to the chirping of the waveguide which conceptually introduces a linear potential. From Figs. 5(a) and 5(d) we can see that the soliton changes its spatial position from the central waveguide ($n = 0$) and leaves behind a plane-wave-like radiation propagating in the opposite direction. The dynamic nature of

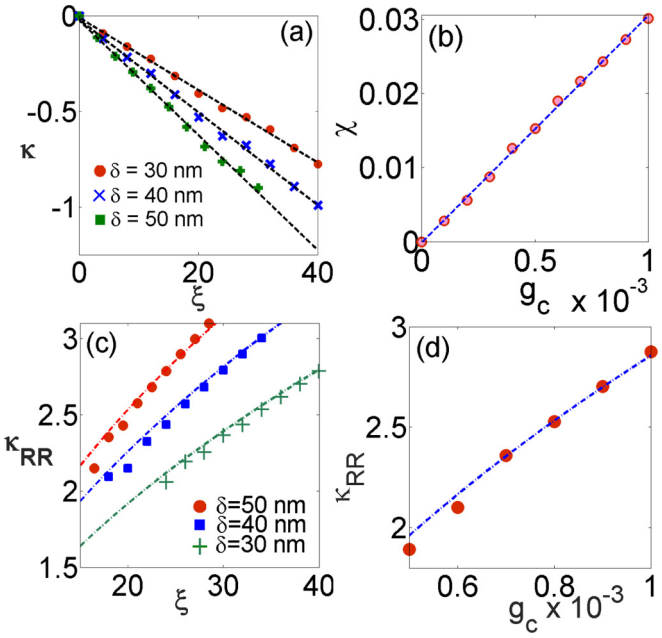

FIG. 6. Position of the soliton and DifRR in the wave-number domain as a function of propagation distance for different values of δ. (b) Evolution of DifRR for different chirp parameters δ. The dotted lines are obtained using the modified PM relation (13).

DifRR is prominent in the (κ, ξ) plane where it shifts along the propagation distance as indicated by the tilted dashed line in Figs. 5(b) and 5(e). The intensity of the generated DifRR and its position (at the κ plane) can be controlled by δ. For higher values of δ, stronger DifRR is generated at relatively shorter propagation distance. The XFROG diagrams in Figs. 5(c) and 5(f) clearly represent the formation of a discrete soliton and DifRR (indicated by arrows). Due to anomalous recoil [19], a part of the DifRR falls on the other side of the Brillouin boundary when the chirp is strong enough (e.g., $\delta > 40$ nm). The variation of the coupling coefficient due to the irregularities in the WA can be approximated as an external potential. However, an equivalent strength of the potential is difficult to extract from the governing equation [Eq. (11)]. In an attempt, numerically we try to extract the relationship between the potential strength (χ) and chirp parameter $(g_c = \delta/d_0)$. In Fig. 6(a) we illustrate the variation of soliton wave number (κ) along propagation distance (ξ), which clearly shows a linear relationship. The slope of the linear variation depends on δ (or g_c).

Inspired by the the variational results, we can propose an approximate equation to describe the evolution of the soliton wave number as

$$\kappa(g_c, \xi) = \kappa_0 - \chi(g_c)\xi, \tag{12}$$

where $\chi(g_c)$ is related to the effective potential arising due to the chirp parameter g_c. The wave-number shift $(\Delta\kappa)$ of the propagating soliton is noted for several g_c, which follows a linear relation. Based on the numerical fit as shown in Fig. 6(b) we establish an empirical relation between potential strength (χ) and chirp parameter (g_c): $\chi(g_c) = m_c g_c$ where the slope is calculated to be $m_c \approx 30$. With this information we can take into account the variation of κ and its dependency on g_c when the soliton propagates through the chirped WA. The change of wave vector leads to a modification of the existing PM equation Eq. (8) where we have to impose the linear variation of the wave number as a function of g_c and propagation distance (ξ). The modified PM equation reads

$$\{\cos(\kappa_{RR}) - \cos[\kappa(g_c, \xi)] + \sin[\kappa(g_c, \xi)]\Delta\kappa\} = \widetilde{\Psi}_0^2 \tag{13}$$

where $\Delta\kappa \equiv \kappa_{RR} - \kappa(g_c, \xi)$. For a simplified analysis, we consider only the evolution of the soliton wave number and compare the position of DifRR obtained from the modified PM equation through Eq. (13) with numerical results. In Fig. 6(c) we demonstrate the evolution of the dynamic DifRR for several δ. The locations of κ_{RR} are obtained numerically by solving the governing equation Eq. (11) and are in good agreement with the modified PM equation Eq. (13). Finally in Fig. 6(c) we demonstrate the variation of κ_{RR} with the chirp parameter g_c at a fixed output ($\xi = 25$). The dotted line is obtained from the modified PM expression Eq. (13), which is in good agreement with numerically simulated data (solid dots).

C. Solitons with an initial nonzero wave number ($\kappa_0 \neq 0$)

In this section, we theoretically and numerically analyze the evolution of a soliton having nonzero initial wave number $(\kappa_0 \neq 0)$ in the linearly chirped WA. The interplay between κ_0 and chirping parameter brings versatility in the soliton dynamics and allows us to investigate the operating domain. The wave vector of the propagating field shifts linearly due to the perturbation imposed by the waveguide chirping. As a consequence, the propagating solitons get self-accelerated, which is also theoretically predicted by variational method. For numerical analysis, we consider a soliton propagation for a fixed chirp value $\delta = 30$ nm. Here we can have two cases, $\kappa_0 < 0$ and $\kappa_0 > 0$. For positive initial wave number $(\kappa > 0)$ we observe a striking feature where the soliton emits twice during its propagation.

In Fig. 7(a) we illustrate the soliton dynamics in n space where the accelerated soliton emits two consecutive radiations marked by numbers 1 and 2. Note Eq. (6), which is not an exact solution for the chirped WA, emits some low-amplitude damped-oscillatory radiation in the form of Airy tails during its acceleration [20,44,45]. The amplitudes of such radiations are weak in comparison with the phase-matched DifRR. In κ space, as shown in Fig. 7(b), the DifRR is prominent and shows its dynamic nature. The first radiation appears at around $\xi \approx 5$ whereas the second begins at $\xi \approx 50$. Figure 7(b) helps us to understand qualitatively the possible reason for dual DifRR. The transverse wave number (κ) of the propagating soliton shifts linearly with a negative slope due to waveguide chirping. For initial positive wave number $(\kappa_0 > 0)$ there will be a crossover when κ shifts from positive to negative value due to continuous wave-number shift. In Fig. 7(b) we can observe this crossover of wave number which occurs around $\xi \sim 30$. With suitable choice of parameter it is possible that the PM equation [Eq. (13)] can be satisfied for $\kappa > 0$ as well as $\kappa < 0$, which leads to two independent radiations. In Fig. 7(c) we capture the spatial spectrogram of the entire dynamics at a fixed distance $\xi = 15$ where the first radiation is evident and the second

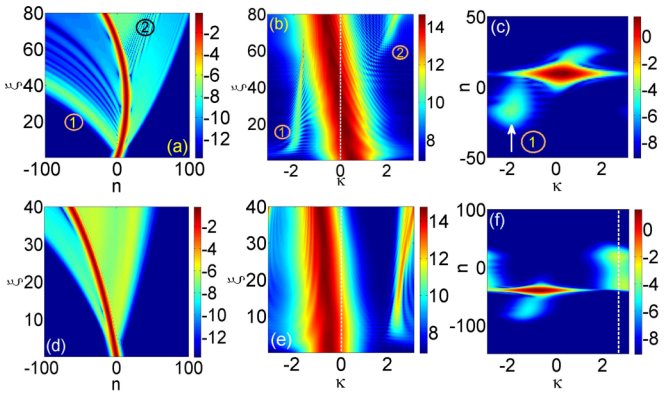

FIG. 7. Discrete soliton propagation in the (a), (d) (n-ξ) and (b), (e) (κ-ξ) plane for $\psi_0 = 0.8$, $\delta = 30$ nm, and $\kappa_0 = 0.5$ (for (a), (b)) and $\kappa_0 = -0.5$ (for (d), (e)). (b) Dual and (e) single DifRR are evident in κ space. A tiny part of the radiation experiences a boundary reflection in κ space and emerges on the other side as a part of anomalous recoil. (c) Spatial spectrogram at $\xi = 20$ where the first DifRR is indicated by the arrow. (f) Spatial spectrogram at $\xi = 40$; the location of the DifRR is indicated by the vertical dotted line.

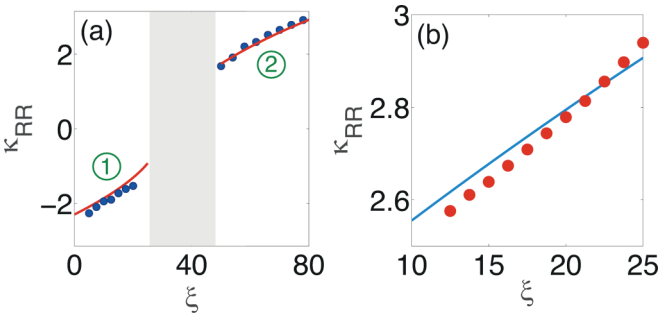

FIG. 8. (a) κ_{RR} as a function of ξ for dual radiation with the parameters $\kappa_0 = 0.5$, $\psi_0 = 0.8$, and $\delta = 30$ nm. The two branches indicate two radiations that appear at two different ranges of distances. (b) κ_{RR} as a function of ξ for single radiation for the parameters $\kappa_0 = -0.5$, $\psi_0 = 0.8$, and $\delta = 30$ nm. In the figures, the solid lines represent the analytical prediction obtained from Eq. (13) where dots are numerical data.

radiation is yet to appear. To visualize the complete picture see Supplemental Material [46].

In Figs. 7(d)–7(f) we demonstrate the complete dynamics of the discrete soliton with negative initial wave number ($\kappa_0 < 0$). Note that, in case of $\kappa_0 < 0$, there is no crossover of the soliton wave number and its value remains negative throughout the propagation. The Airy tail emitted from the soliton as a pedestal is weak and diminishes during propagation. Under such condition only one solution appears from Eq. (13) and we observe a single strong DifRR. The soliton and the detuned wave number of the generated DifRR are well separated in the κ space exhibiting a dynamic evolution [see Fig. 7(e)]. The generated DifRR is moving away from the soliton owing to the effective linear potential induced by the chirp. However, due to the boundary of $-\pi$ to π set by the one-dimensional lattice, the DifRR emerges from the other side due to anomalous recoil by undergoing a phase shift of 2π. In Fig. 7(f) we demonstrate the spatial spectrogram where DifRR is evident and indicated by a vertical dotted line. A weak Airy tail is visible in the spectrogram the wave number of which overlaps with the soliton. From Fig. 7(f) we also have the hint of anomalous recoil which appears at the Brillouin boundary. Finally in Fig. 8 we demonstrated the evolution of DifRR theoretically supported by Eq. (13) (solid lines). The dual radiation is evident in Fig. 8(a) for $\kappa_0 > 0$ where the soliton emits twice. Two distinct solutions appear when we take into account the crossover of the wave number (κ) in the PM equation [Eq. (13)]. The shaded region indicates no radiation zone. The solid dots in Fig. 8(a) represent the values of κ_{RR} extracted from the numerical solution of Eq. (11). In Fig. 8(b) we depict the case for $\kappa < 0$ where a single strong radiation is emitted from the moving soliton. The soliton wave number (κ) remains negative throughout the propagation and leads to a single solution of Eq. (13). The analytical solution (solid line) based on the PM equation [Eq. (13)] quantitatively determines the radiation wave numbers and corroborates well with the numerical values of κ_{RR} indicated by solid dots in Fig. 8.

IV. CONCLUSION

We demonstrate that a linearly chirped waveguide array exhibits discrete-soliton mediated dynamic diffractive resonance radiation where the wave number of the radiation field shifts along propagation distance. Perturbation due to irregularities of waveguide arrangements is modeled as a linear potential in a nonlinear Schrödinger equation which governs the soliton dynamics. We propose realistic waveguide design where diffractive resonance radiation can be excited naturally from a discrete soliton. To gain intuitive insight into soliton evolution inside a transversely chirped WA we exploit perturbative variational analysis. The variational treatment leads to the equations of motion of soliton parameters which predict self-acceleration of discrete solitons and linear wave-number shift. Using this information we model the discrete nonlinear Schrödinger equation and theoretically modify the phase-matching equation, which capture the dynamic nature of wave-number shift of diffractive radiation. Evolution of the soliton is investigated for zero and nonzero initial wave numbers. An intriguing effect of dual diffractive resonance radiation is observed when a soliton with positive wave number is launched in the WA. The theoretical underpinning of dual radiation lies with the fact that the soliton wave number experiences a crossover by shifting its value from positive to negative owing to the chirping in the WA. This crossover results in two distinct solutions of the PM equation at two different propagation distances and leads to dual radiation. We theoretically confirm this phenomenon by solving the modified PM equation. This paper could pave the way for designing waveguide-array based optical devices that are capable of generating a controllable spatial supercontinuum.

ACKNOWLEDGMENT

A.P.L. acknowledges University Grants Commission, India for support through Junior Research Fellowship in Sciences, Humanities and Social Sciences (ID 515364).

[1] H. Haus and L. Molter-Orr, IEEE J. Quantum Electron. **19**, 840 (1983).

[2] T. Pertsch, T. Zentgraf, U. Peschel, A. Bräuer, and F. Lederer, Phys. Rev. Lett. **88**, 093901 (2002).

[3] A. B. Aceves, C. De Angelis, T. Peschel, R. Muschall, F. Lederer, S. Trillo, and S. Wabnitz, Phys. Rev. E **53**, 1172 (1996).

[4] H. S. Eisenberg, Y. Silberberg, R. Morandotti, A. R. Boyd, and J. S. Aitchison, Phys. Rev. Lett. **81**, 3383 (1998).

[5] F. Lederer, G. I. Stegeman, D. N. Christodoulides, G. Assanto, M. Segev, and Y. Silberberg, Phys. Rep. **463**, 1 (2008).

[6] Y. S. Kivshar and D. K. Campbell, Phys. Rev. E **48**, 3077 (1993).

[7] R. Morandotti, U. Peschel, J. S. Aitchison, H. S. Eisenberg, and Y. Silberberg, Phys. Rev. Lett. **83**, 4756 (1999).

[8] Y. Lahini, A. Avidan, F. Pozzi, M. Sorel, R. Morandotti, D. N. Christodoulides, and Y. Silberberg, Phys. Rev. Lett. **100**, 013906 (2008).

[9] F. Dreisow, A. Szameit, M. Heinrich, T. Pertsch, S. Nolte, A. Tünnermann, and S. Longhi, Phys. Rev. Lett. **102**, 076802 (2009).

[10] F. Dreisow, M. Heinrich, R. Keil, A. Tünnermann, S. Nolte, S. Longhi, and A. Szameit, Phys. Rev. Lett. **105**, 143902 (2010).

[11] T. X. Tran, S. Longhi, and F. Biancalana, Ann. Phys. (NY) **340**, 179 (2014).

[12] A. Marini, S. Longhi, and F. Biancalana, Phys. Rev. Lett. **113**, 150401 (2014).

[13] C. R. Rosberg, I. L. Garanovich, A. A. Sukhorukov, D. N. Neshev, W. Krolikowski, and Y. S. Kivshar, Opt. Lett. **31**, 1498 (2006).

[14] Y. V. Kartashov, V. A. Vysloukh, and L. Torner, J. Opt. Soc. Am. B **22**, 1356 (2005).

[15] M. I. Molina, Y. V. Kartashov, L. Torner, and Y. S. Kivshar, Opt. Lett. **32**, 2668 (2007).

[16] L. Verslegers, P. B. Catrysse, Z. Yu, and S. Fan, Phys. Rev. Lett. **103**, 033902 (2009).

[17] R.-C. Shiu, Y.-C. Lan, and C.-M. Chen, Opt. Lett. **35**, 4012 (2010).

[18] B. Wang, H. Huang, K. Wang, H. Long, and P. Lu, Opt. Lett. **39**, 4867 (2014).

[19] T. X. Tran and F. Biancalana, Phys. Rev. Lett. **110**, 113903 (2013).

[20] D. V. Skryabin and A. V. Gorbach, Rev. Mod. Phys. **82**, 1287 (2010).

[21] U. Peschel, T. Pertsch, and F. Lederer, Opt. Lett. **23**, 1701 (1998).

[22] T. Pertsch, P. Dannberg, W. Elflein, A. Bräuer, and F. Lederer, Phys. Rev. Lett. **83**, 4752 (1999).

[23] L. Martin, G. D. Giuseppe, A. Perez-Leija, R. Keil, F. Dreisow, M. Heinrich, S. Nolte, A. Szameit, A. F. Abouraddy, D. N. Christodoulides, and B. E. A. Saleh, Opt. Express **19**, 13636 (2011).

[24] S. P. Stark, A. Podlipensky, and P. S. J. Russell, Phys. Rev. Lett. **106**, 083903 (2011).

[25] Z. Chen, A. J. Taylor, and A. Efimov, Opt. Express **17**, 5852 (2009).

[26] F. Arteaga-Sierra, C. Milián, I. Torres-Gómez, M. Torres-Cisneros, A. Ferrando, and A. Dávila, Opt. Express **22**, 2451 (2014).

[27] A. Roggenbuck, K. Thirunavukkuarasu, H. Schmitz, J. Marx, A. Deninger, I. C. Mayorga, R. Güsten, J. Hemberger, and M. Grüninger, JOSA B **29**, 614 (2012).

[28] J. Travers and J. Taylor, Opt. Lett. **34**, 115 (2009).

[29] S. Roy, S. K. Bhadra, and G. P. Agrawal, Opt. Lett. **34**, 2072 (2009).

[30] H. Guo, C. Herkommer, A. Billat, D. Grassani, C. Zhang, M. H. Pfeiffer, W. Weng, C.-S. Bres, and T. J. Kippenberg, Nat. Photonics **12**, 330 (2018).

[31] R. Morandotti, U. Peschel, J. S. Aitchison, H. S. Eisenberg, and Y. Silberberg, Phys. Rev. Lett. **83**, 2726 (1999).

[32] A. A. Sukhorukov, Y. S. Kivshar, H. S. Eisenberg, and Y. Silberberg, IEEE J. Quantum Electron. **39**, 31 (2003).

[33] D. N. Christodoulides and R. I. Joseph, Opt. Lett. **13**, 794 (1988).

[34] F. Lederer and Y. Silberberg, Opt. Photon. News **13**, 48 (2002).

[35] H. S. Eisenberg, Y. Silberberg, R. Morandotti, and J. S. Aitchison, Phys. Rev. Lett. **85**, 1863 (2000).

[36] T. X. Tran and F. Biancalana, Opt. Express **21**, 17539 (2013).

[37] C. M. de Sterke, J. N. Bright, P. A. Krug, and T. E. Hammon, Phys. Rev. E **57**, 2365 (1998).

[38] G. P. Agrawal, *Nonlinear Fiber Optics*, 5th ed. (Elsevier, Amsterdam, 2013).

[39] A. A. Sukhorukov, Phys. Rev. Lett. **96**, 113902 (2006).

[40] A. Szameit, D. Blömer, J. Burghoff, T. Pertsch, S. Nolte, and A. Tünnermann, Appl. Phys. B **82**, 507 (2006).

[41] I. Pavlov, O. Tokel, S. Pavlova, V. Kadan, G. Makey, A. Turnali, O. Yavuz, and F. O. Ilday, Opt. Lett. **42**, 3028 (2017).

[42] R. Tewari and K. Thyagarajan, J. Lightwave Technol. **4**, 386 (1986).

[43] A. W. Snyder, J. Opt. Soc. Am. **62**, 1267 (1972).

[44] A. V. Gorbach and D. V. Skryabin, Opt. Express **16**, 4858 (2008).

[45] A. C. Judge, O. Bang, and C. M. de Sterke, JOSA B **27**, 2195 (2010).

[46] See Supplemental Material at http://link.aps.org/supplemental/10.1103/PhysRevA.102.033512 for a spatial spectrogram movie describing the evolution of the soliton and the generation of the dual radiation successively along the propagation direction.